Mechanical Systems and Signal Processing 149 (2021) 107324

Contents lists available at ScienceDirect

Mechanical Systems and Signal Processing

journal homepage: www.elsevier.com/locate/ymssp

An active meta-layer for optimal flexural wave absorption and cloaking

Xiaopeng Li [a], Yangyang Chen [a,*], Rui Zhu [b], Guoliang Huang [a,*]

[a] Department of Mechanical & Aerospace Engineering, University of Missouri, Columbia, MO 65211, USA
[b] School of Aerospace Engineering, Beijing Institute of Technology, Beijing 100081, China

ARTICLE INFO

Article history:
Received 5 July 2020
Received in revised form 31 August 2020
Accepted 23 September 2020

Keywords:
Meta-layer
Absorber
Broadband vibration control
Cloaking

ABSTRACT

Flexural wave propagation is common in thin structures and plays a key role in vibrations of structures. Designs of flexural wave absorbers for vibration control have been constantly pursued for decades aiming to find structures that can best balance tradeoffs between small sizes or lightweights and broadband operations. However, their absorption performance has long been evaluated on a case-by-case basis, and the theoretical limit characterizing the relationship between the absorption spectrum and the sample thickness and mass density is missing. In this study, by adopting an inequality as its electromagnetism and acoustics counterparts, the theoretical limit of flexural wave absorption is established. An active meta-layer composed of piezoelectric sensors and actuators with feedback control loops is proposed for optimal wave absorption. We experimentally demonstrate the active meta-layer for optimal broadband wave and vibration control in the beam and acting as skin cloaks of large voids in the plate. The active meta-layer is electrically programmable and scalable without losing stability. The approach proposed sheds light on designs of reconfigurable dynamic control devices and enables alternative solutions for ultrasonic sensing of complex engineering structures.

1. Introduction

Acoustic/elastic metamaterials that are made by specific geometries in their microstructures display a range of unusual dynamic effective material properties absent from naturally occurring materials [1–13]. During the past two decades, acoustic/elastic metamaterials have been extensively exploited in lots of wave and vibration control applications, which include but not limited in elastic wave/vibration attenuation and absorption [4–8], cloaking of flexural vibrations in a structured plate [9], elastic waveguiding through sharp turns [10,11], the parity-time symmetric material system with gain and loss components for cloaking purpose [12,13], and controllable and tunable wave manipulations [14–18]. On one hand, they have demonstrated efficient or nearly perfect solutions to those applications. On the other hand, they require repeated unit cells for metamaterials exhibiting their effective properties, which, unfortunately, usually involve bulky and complex geometries and/or control systems.

Metasurfaces, a kind of metamaterials with reduced dimensions, have recently emerged as a powerful approach for transforming waves [19–27]. Metasurfaces are designed by arranging suitable material discontinuities on an interface to produce desired wave scattering effects. The significantly reduced number of constitutive units and occupied spaces make

* Corresponding authors.
E-mail addresses: yc896@mail.missouri.edu (Y. Chen), huangg@missouri.edu (G. Huang).

https://doi.org/10.1016/j.ymssp.2020.107324
0888-3270/

metasurfaces excellent substitutes for bulk metamaterials. The concept of metasurfaces has found a lot of interesting and unconventional applications in wave/vibration isolation and absorption [19–21], wave redirecting [22–26], real-time and reconfigurable wave manipulation [27], and cloaking [27]. Inspired by this concept, in the study, we suggest a type of metasurfaces with active control systems, which we call active meta-layers. We show the active meta-layers can support two unprecedented wave control functions: "Optimal" flexural wave absorption and cloaking.

A short and qualitative description of the "Optimal" flexural wave absorption is that a structure can achieve the largest absorption coefficients in the broadest operational spectrum but with minimum weight and/or least thickness. However, a quantitative description of "Optimal" is still absent. Once the weight and/or thickness of a structure are fixed, what the largest absorption coefficients and how broad the operational spectrum can be achieved? This theoretical limit balancing tradeoffs among those quantities has been overlooked for decades. Even though given the fact that mechanical wave absorbers are important components for ensuring safety and reliability of a wide variety of structures, and existing wave absorbing materials or structures have been widely explored (i.e. tuned mass dampers [28,29], highly damped materials [30,31], gradient index materials or structures [32–36], and active structures based on feedforward or feedback control loops [37–40].). Unfortunately, in previous studies, their overall performance has only been evaluated on a case-by-case basis, lacking a uniformed and normalized criterion.

Here, by adopting an inequality dictated by causality as its electromagnetism and acoustics counterparts [41,42], we establish a theoretical limit of flexural wave absorption to characterize the relation of the absorption spectrum and the sample thickness as well as mass density. The relation is interpreted by the inequality which produces the least thickness and density to the absorption coefficient and its bandwidth ratio achievable for a physically realizable mechanical wave absorber. To pursue this theoretical limit, wave absorbers are required to be frequency-dependent and highly flexible over a large frequency band, which is difficult to be realized with passive structures. Recently, active metasurfaces with piezoelectric sensors and actuators connected by electrical circuits are studied to redirect and reconfigure mechanical waves in real-time, which makes them the best candidate for designing optimal wave absorption [27].

In light of those considerations, we propose a design of active meta-layers in elastic beams and plates for optimal flexural wave absorptions. The active meta-layer consists of piezoelectric sensors and actuators connected with feedback electrical control loops. We numerically and experimentally demonstrate its optimal wave absorption performance and broadband vibration attenuation by systematically designing a second-order electrical transfer function in the feedback control loop. We find the thickness of the meta-layer is close to the minimum value as dictated by causality. The meta-layer is finally employed to construct a unidirectional skin cloak of large voids in a plate through combinations with the active actuation.

2. The theoretical limit of flexural wave absorption

When designing flexural wave absorbers, the ultimate goal is to find damping materials or structures that can absorb waves close to their theoretical limits, i.e. absorbers with thickness, d, or weight, m, possess the lowest reflectance at broadest frequency spectrum (Fig. 1(a)). To achieve this goal, metamaterials with complex effective bending stiffness and/or mass density in particular forms of frequency become a natural choice. Thanks to causality, however, real and imaginary parts of the bending stiffness or mass density of any materials cannot be arbitrary functions of frequency, instead, they are correlated with each other by Kramers–Kronig relations [43,44]. This relation can be translated into an inequality relating the absorption coefficient to the thickness of the absorbing material. The inequality has been widely applied in electromagnetism and acoustics [41,42], but rarely adopted and defined in elasticity.

Here, we extend this relation to flexural wave absorbers with free boundaries. Consider a flexural wave absorber with the thickness, d, and effective static mass density per unit length, ρ_s (see Fig. 1(a)), attached to one end of a host beam. The other end of the absorber is free. Let the complex reflection coefficient, r, be an analytical function of complex frequencies, ω. If the time-dependent transverse displacement field can be expressed in function of the lower half-plane of complex frequencies. The reflection coefficient, r, can be a function of the wavelength, λ, such that r has no poles in the upper half-plane of complex wavelengths, but may have zeros there. Then the ancillary function can be written as [41,42]

$$\bar{r}(\lambda) = r(\lambda)\prod_n \frac{\lambda-\lambda_n^*}{\lambda-\lambda_n} \tag{1}$$

where λ_n denotes zeros located in the upper half-plane of complex wavelengths, satisfying $\mathrm{Re}(\lambda_n) = 0$, and * represents a complex conjugate. Consider the fact that the logarithm of $\bar{r}(\lambda)$ is an analytic function in the upper half-plane of complex wavelengths. The Cauchy theorem is valid [41,42], which states that the integration over any closed contour yields zero if the contour C is located within the upper half-plane of λ. Let the contour consist of the whole axis of real wavelengths and the closing semicircle C_∞, which belongs to the upper half-plane and has an infinite radius. The real part of the Cauchy integral transforms to [41,42]

$$Re\left(\int_C \ln\bar{r}\,d\lambda\right) = 2\int_0^\infty \ln|r|d\lambda + Re\left(\int_{C_\infty}\ln r d\lambda\right) + Re\left(\sum_n\int_{C_\infty}\ln\frac{\lambda-\lambda_n^*}{\lambda-\lambda_n}d\lambda\right) = 0. \tag{2}$$

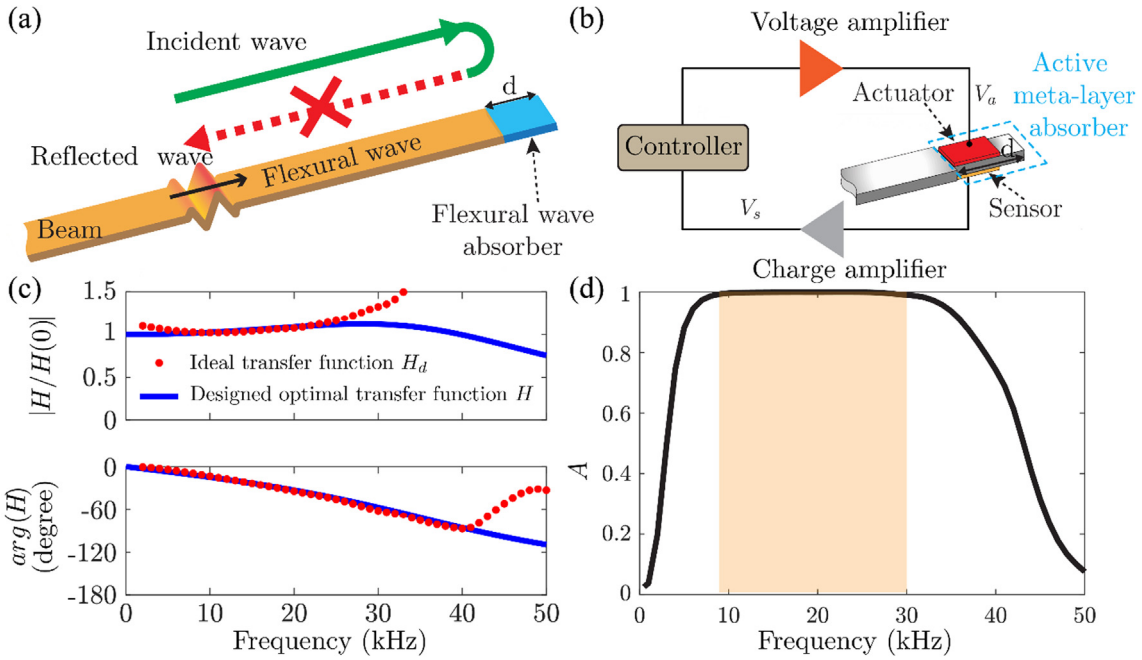

Fig. 1. (a) Schematic of a broadband flexural wave absorber. Broadband reflected waves are inhibited due to the presence of the absorber. (b) Design of the active meta-layer absorber. (c) Frequency responses of the ideal transfer function H_d at discrete frequencies and optimal causal transfer function H implemented into the active meta-layer. Normalized magnitudes and phase angles are shown. (d) Numerically calculated absorption coefficients of the active meta-layer implemented with the optimal transfer function H.

We first calculate the second term on the right-hand side of Eq. (2). The reflection coefficient needs to be expressed at the limit of the infinite wavelength. Consider time-harmonic flexural waves propagated along the host beam. The total displacement wave field can be written as

$$w = A^+ e^{ikx} + A^- e^{-ikx} + \bar{A} e^{kx} \tag{3}$$

where the wavenumber $k = (\rho_0 \omega^2 / D_0)^{1/4}$ with ρ_0 and D_0 representing the mass density per unit length and bending stiffness of the host beam, respectively, A^+, A^- and $\bar{A}$ denote the complex wave amplitudes of right-, left-propagated and evanescent waves, respectively. The time-harmonic term $e^{-i\omega t}$ is dropped from Eq. (3). When the wavelength approaches infinity, the flexural wave absorber can be assumed as a point mass attached to the end of the host beam. At this boundary, the bending moment equals to zero and the equilibrium between the shear force and linear momentum of the point mass leads to

$$A^+ + A^- = \bar{A}, D_0\left(-ik^3 A^+ + ik^3 A^- + k^3 \bar{A}\right) = \omega^2 \rho_s d\left(A^+ + A^- + \bar{A}\right) \tag{4}$$

From Eq. (4), the reflection coefficient reads

$$r = \frac{A^-}{A^+} = i + \frac{2\pi(1-i)\rho_s d}{\rho_0 \lambda}. \tag{5}$$

Using Eq. (5), the second term on the right-hand side of Eq. (2) finally becomes

$$Re\left(\int_{C_\infty} \ln r d\lambda\right) = \lim_{R\to+\infty} Re\left[\int_0^\pi \ln\left(i + \frac{2\pi(1-i)\rho_s d}{\rho_0 r e^{i\theta}}\right) d\theta\right] = \frac{2\pi^2 \rho_s d}{\rho_0}. \tag{6}$$

Furthermore, the third term on the right-hand side of Eq. (2) can be simplified as

$$Re\left(\sum_n \int_{C_\infty} \ln \frac{\lambda - \lambda_n^*}{\lambda - \lambda_n} d\lambda\right) = -2\pi \sum_n Im(\lambda_n). \tag{7}$$

Consequently, Eq. (2) can be rewritten as

$$\int_0^\infty \ln|r| d\lambda = -\frac{\pi^2 \rho_s d}{\rho_0} + \pi \sum_n Im(\lambda_n). \tag{8}$$

Since all λ_n are in the upper half-plane, $\mathrm{Im}(\lambda_n)$ in the second term of the right-hand side of Eq. (8) have a positive sign. Therefore,

$$\left|\int_0^\infty ln|r(\lambda)|d\lambda\right| \le \frac{\pi^2\rho_s d}{\rho_0}. \tag{9}$$

Alternatively,

$$\left|\int_0^\infty ln[1-A(\lambda)]d\lambda\right| \le \frac{2\pi^2\rho_s d}{\rho_0}, \tag{10}$$

where A denotes the absorption coefficient. Eq. (10) introduces the theoretical limit of absorption of any flexural wave absorbers, where the integral of the absorption coefficient has an upper bound proportional to the product of the thickness of the absorber and the mass density ratio between the absorber material and background beam. Note that perfect absorption ($A = 1$) can only happen at discrete frequencies and broadband absorption cannot be exactly perfect ($A \neq 1$). Therefore, to design optimal broadband flexural wave absorbers, one needs to carefully balance between wave absorption and operational bandwidth to approach the theoretical limit.

3. Design of an optimal active meta-layer

In this section, we suggest such an optimal design of active meta-layers based on piezoelectric shunting. This active approach is capable of not only flexibly tailoring the absorption spectrum without varying geometries but also approximately reaching the theoretical limit of flexural wave absorption. We construct the meta-layer by cutting one end of a host beam into a narrower beam and attaching two piezoelectric patches with the same dimension on the upper and lower surfaces of this narrower beam (Fig. 1(b)). Two piezoelectric patches are bonded symmetrically with respect to the neutral plane of the beam, and adjacent to the edges of the cuts (Fig. 1(b)). The geometric and material parameters can be found in Tables 1 and 2, respectively. In the design, the lower patch functions as a sensor to detect the local bending curvature, and the upper patch acts as an actuator to generate the bending moment at the location it attached. The sensor and actuator are connected by an electrical circuit. The output and input signals of the circuit, V_a and V_s, are controlled by a transfer function, $H = V_a/V_s$. When an incident wave impinges to the meta-layer, the sensor will sense a signal due to changes of the local bending curvature, and the actuator controlled by the transfer function will in turn generate the bending moment response and emit an additional wave to the background beam in a destructive manner. The additional wave then interferes with the reflected background wave.

To derive the relations between the transfer function H and wave reflection coefficient r, we consider a meta-layer attached on one end of a host beam as shown in Fig. 1(b). Assuming incident waves coming from the left and propagate to the meta-layer, the displacement wave field of an incident wave can be written as

$$w_{in} = w_0 e^{ikx}. \tag{11}$$

When the meta-layer is disconnected from the circuits, the incident wave will be totally reflected at the free boundary of the meta-layer, where the passive refection coefficient reads $r_0 = w_r^{(0)}/w_0$ with $w_r^{(0)}$ being the amplitude of the reflected wave. Applying a voltage, V_a, on the piezoelectric actuator in the meta-layer, it generates right-propagative waves, the amplitude of which can be written as

$$w_a = V_a\kappa_a, \tag{12}$$

where κ_a denotes the effective electromechanical coupling coefficient of the actuator. On the other hand, the sensing voltage from the piezoelectric sensor in the meta-layer contains two components: one is induced by the incident wave; the other is produced due to the actuator-to-sensor feedback effect. Therefore, the sensing voltage can be express by

Table 1
Geometric parameters of the optimal active meta-layer.

Flexural wave absorption with active meta-layer							
L	600 mm	L_{PML}	100 mm	L_1	100 mm	L_2	250 mm
L_p	13 mm	w_p	9 mm	h_p	1 mm	h_b	3 mm
w_b	13 mm	d	20 mm				
Reconfigurable structures							
L_{rs}	214 mm	w_1	10 mm	t_1	3 mm	t_w	1 mm
θ_1	60°	θ_1	30°	a_1	10 mm	a_2	5 mm
Cloaking							
R_1	70.76 mm	R_2	90.76 mm	d_1	100 mm	d_2	200 mm
d_3	160 mm						

Table 2
Material properties of the optimal active meta-layer.

Material properties (Steel)					
E	205 GPa	ν	0.28	ρ_b	7850.0 kg/m^3
Material properties (Aluminum)					
E	70 GPa	ν	0.33	ρ_b	2700.0 kg/m^3
Material properties (PZT 5H)					
s_{11}^E	16.5×10^{-12} m^2/N	d_{33}	593×10^{-12}C/N		
s_{33}^E	20.7×10^{-12} m^2/N	d_{31}	-274×10^{-12}C/N		
s_{44}^E	43.5×10^{-12} m^2/N	d_{15}	741×10^{-12}C/N		
s_{12}^E	-4.78×10^{-12} m^2/N	ε_{33}^S	1433.6 ε_0		
s_{13}^E	-8.45×10^{-12} m^2/N	ε_{11}^S	1704.4 ε_0		
ρ_p	7500.0 kg/m^3	ε_0	8.842×10^{-12}C/mV		

$$V_s = V_{sb} + V_{fb} = w_0\kappa_s + GV_a, \tag{13}$$

where κ_s denotes the effective electromechanical coupling coefficient of the sensor, and G represents the feedback transfer function. Finally, the transfer function H relates the sensing and actuating voltages by

$$H = \frac{V_a}{V_s}. \tag{14}$$

Combining Eqs. (12)–(14), the reflection coefficient r can be derived as

$$r = \frac{w_a + w_r^{(0)}}{w_0} = \frac{H\kappa_a\kappa_s}{1 - HG} + r_0. \tag{15}$$

As can be found from Eq. (15), the wave reflection (absorption) coefficient, r (A), can be controlled by the transfer function, H.

To achieve optimal wave absorption (near or at the theoretical limit), we conduct a series of numerical studies for calculating the optimal transfer function, H. Firstly, for perfect absorption ($A = 1$) at discrete frequencies, amplitudes, and phase angles of the transfer function at some discrete frequencies from 2 to 50 kHz are retrieved and plotted in Fig. 1(c) by red dots. We characterize this discrete transfer function as an ideal transfer function, H_d, which usually cannot be physically realized in the time domain. Numerical procedures for calculating the ideal transfer function can be found in Appendix A. From Fig. 1(c), we find the amplitude of the ideal transfer function, H_d, gradually decreases and then increases, when the frequency increases. The phase angle shows a similar trend but with the turning point around 40 kHz, due to the Fabry–Pérot resonance in the meta-layer at this frequency.

Next, to find a real transfer function which can be implemented into the meta-layer for optimal wave absorption, we consider the following criteria: the optimal transfer function should (1) be physically realizable, satisfy causality, and (2) have frequency responses as close as possible to the profiles of the ideal transfer function in both amplitude and phase angle, and (3) the entire electromechanical system (active meta-layer on a host beam) must be stable in the time domain. With these considerations, we formulate an analytical form based on a second-order low-pass filter as the optimal transfer function, $H = \frac{\omega_0^2}{s^2 + 2\zeta\omega_0 s + \omega_0^2}$, where $s = i\omega$ and ω_0 and ζ are the two parameters to be determined. In the design, the frequency range from 5 to 25 kHz is selected as the target to have nearly perfect absorption. Applying the Multivariable Output Error State Space (MOESP) algorithm, we find values of the two optimal parameters in the transfer function, which are $\omega_0 = 2\pi \times 40.8 \times 10^3 1/s$ and $\zeta = 0.517$. Amplitudes and phase angles of this optimal transfer function are also shown in Fig. 1(c) as blue solid curves. Here, we find they align very well with those of the ideal transfer function at frequencies from 5 to 25 kHz.

Stability is then carefully considered and analyzed. We first perform different sets of numerical simulations to determine the ideal transfer functions of meta-layers, when the piezoelectric sensor and actuator are placed on different locations. The operational frequency range of nearly perfect absorption is pre-selected (5–25 kHz), based on which we conduct an optimization procedure to search the optimal transfer functions that will be implemented into the meta-layer. We then look at those optimal transfer functions with the piezoelectric sensor and actuator placed at different locations, and select the best optimal transfer functions based on the two criteria considering the system's stability: (1) The optimal transfer function should lack a strong resonance peak near ω_0. This is because strong responses of the transfer function can easily make the feedback system divergence. Quantitative studies can be performed according to Nyquist criteria [7]. The first criterion indicates that the damping ratio ζ cannot be too small. (2) The transfer function response near 40 kHz should be weak enough, as the Fabry–Pérot resonance is around this frequency, which produces strong responses in the feedback loop. The second criterion implies that the damping ratio ζ cannot be too large. Based on those considerations, we select several locations of the piezoelectric sensor and actuator and their corresponding optimal transfer functions. To further validate those designs, we perform time-domain analyses and find an active meta-layer that can be stable over a long enough time.

We then conduct numerical simulations to examine the wave absorption performance of the active meta-layer with this optimal transfer function. Fig. 1(d) shows the absorption coefficient, A, of this design at different frequencies. It can be seen that waves with frequencies from 9 to 30 kHz (orange shadow area) can be nearly totally absorbed with $A \geq 99\%$. This provides strong evidence on the effectiveness of the design principle and optimization approach. Furthermore, we define a ratio, $A_p = \frac{\left|\int_0^\infty ln[1-A(\lambda)]d\lambda\right|\rho_0}{2\pi^2\rho_s d}$, to characterize the flexural wave absorption performance of an absorber. When $A_p = 1$, the absorber is considered perfectly optimal at its theoretical limit. Through calculations using the data shown in Fig. 1(d), we find $A_p \approx 0.85$ for the current meta-layer design. The performance can be further improved through incorporating materials displaying passive damping into the active meta-layer or conducting optimizations on geometries of piezoelectric patches. The optimal meta-layer presented here is only from the optimizations on the electrical transfer function.

Note that the design of a meta-layer for optimal wave absorption in different structures typically includes two procedures: (1) selection of dimensions and geometries; and (2) selection of proper electrical transfer functions, which are intrinsically coupled. That means the electrical transfer functions should be changed if the dimensions and geometries of the meta-layer are modified or vice versa. Given the fact that the optimal solution of geometric and electrical parameters is neither unique nor arbitrary. Geometries of the meta-layer could have constraints for some practical applications. For example, to design this meta-layer in a beam, locations of the sensor and the actuator is an important parameter that should be within a small range to ensure system stability. Whereas, other geometric parameters, such as dimensions of the beam and piezoelectric sensor and actuator patches would have much wider choices. Overall, the proposed approach with special dimensions can limit some practical applications. However, that should only be in a small portion.

4. Experimental testing

We fabricate the active meta-layer at one end of a steel host beam and test its wave absorption performance with the optimal transfer function. Illustration of the fabricated sample and experimental setup is shown in Fig. 2(a). To fabricate the meta-layer, we first cut one end of the host beam into a narrower beam using a fiber laser cutting machine and attach two piezoelectric patches produced by STEMiNC (SM112; Dimensions: 13 mm × 9 mm × 1 mm). They are bonded on the top and bottom surfaces of the cut beam using conductive epoxy (Chemtronics).

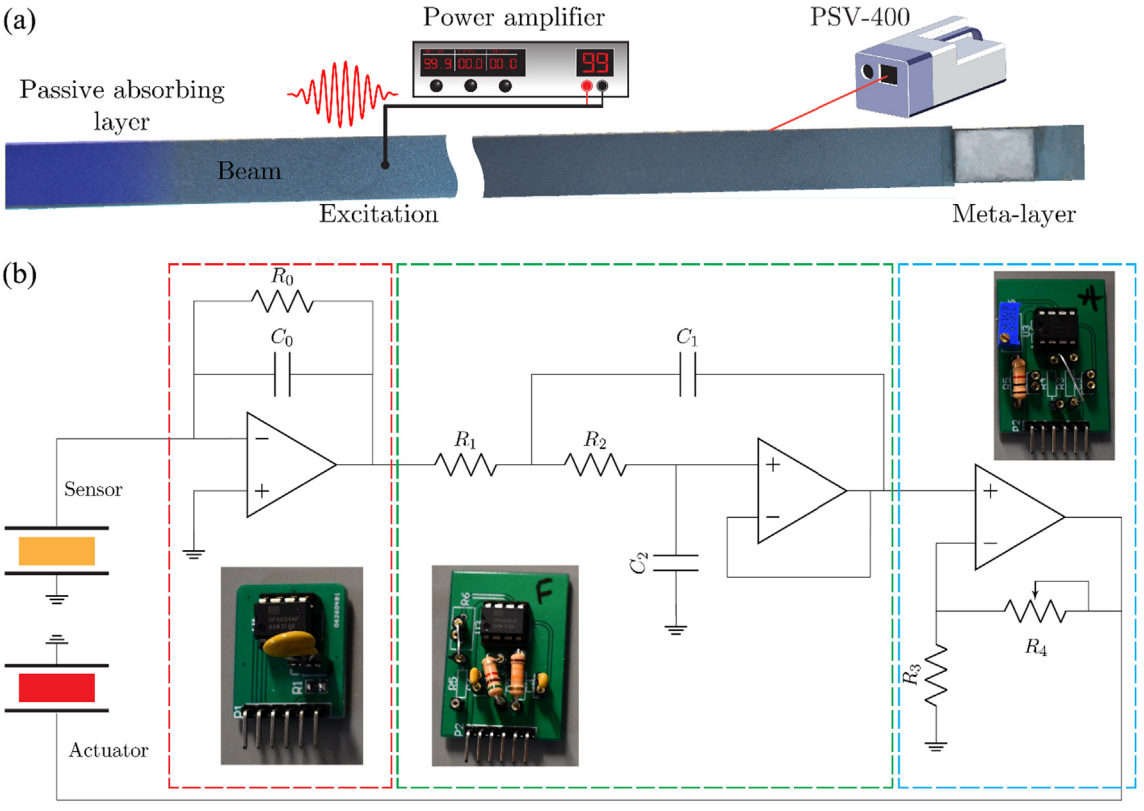

Fig. 2. (a) Experimental setup of the meta-layer for wave absorption tests. (b) The circuit diagram and fabricated circuits.

The control circuit of an active meta-layer consists of three basic components: a charge amplifier, a second-order low-pass filter, and a voltage amplifier. The circuit diagram and corresponding fabricated circuits are shown in Fig. 2(b). In the charge amplifier, we select the reference capacitance $C_0 = 2$ nF. For the second-order low-pass filter, $R_1 = 12$ kΩ, $R_2 = 5.1$ kΩ, C_1=1nF and C_2 = 220 pF. In the voltage amplifier, a reference resistor ($R_3 = 1$ kΩ) and a potentiometer are used to adjust the amplification ratio. All those analog circuits are fabricated on a portable printed circuit board (PCB). It may need to mention that a digital controller can also be applied to compose the second-order low-pass filter as well.

One piezoelectric transducer is attached in the middle portion of the host beam to generate incident flexural waves propagating to the meta-layer. Incident wave signals applied on the transducer are generated by an arbitrary waveform generator (Tektronix AFG3022C) and amplified by a high voltage amplifier (Krohn-Hite). Ten-peak tone-burst signals with different central frequencies are employed in the tests. We implement a thick layer of passive absorbing material (Loctite fun-task mounting putty) at the other end of the host beam to suppress unnecessary boundary reflection. The total length of the host beam is 2 m and the length of the passive absorbing layer is about 200 mm. The out-of-plane velocity wave field is measured and recorded by a scanning laser Doppler vibrometer (Polytec PSV-400).

5. Results and discussion

5.1. Optimal flexural wave absorption

Fig. 3(a) shows the measured time-domain signals from the host beam when the control circuit is turned ON (red dotted curves) and OFF (blue solid curves). The central frequency of the incident wave is selected at 10, 15, 20, and 25 kHz, respectively. It can be found from the figure that waves are totally reflected when the control circuit is turned OFF, and the meta-layer behaves as a free boundary. When the control circuit is turned ON, reflected waves from the meta-layer nearly disappear, demonstrating the predicted absorbing effect. We then calculate absorption coefficients based on experimental data and compare them with those from numerical simulations. We plot the percentage error by $\chi = \frac{A_e - A_n}{A_n}$ in Fig. 3(b), where A_e and A_n denote absorption coefficients calculated using experimental and numerical data, respectively. It can be clearly evidenced that experimental and numerical results agree very well with errors below 4%.

5.2. Broadband vibration attenuation

We then test the meta-layer for broadband vibration suppression. The meta-layer is installed at one end of a host beam, which has the other end fixed (Fig. 4(a)). The total length of the cantilever beam is 1 m and the rest of the parameters are the same as for flexural wave absorption case. The host beam is excited by a piezoelectric transducer bonded next to the root of it. Sine modulated-chirp signals with frequencies covering from 5 to 30 kHz are applied to the piezoelectric transducer. The out-of-plane vibration signal is measured from the host beam, 5 mm away from the meta-layer, using a laser vibrometer. Fig. 4(b) shows frequency response functions of measured signals with the control circuit in the meta-layer turned ON and OFF. We find almost all the strong resonance peaks of the beam without the control are inhibited by the meta-layer from 5 to 30 kHz, which aligns very well with the findings in the wave propagation test. It should be noticed that, at frequencies around 8 and 14 kHz, the vibration attenuation is weak, which is mainly caused by the strong rotational motion excited by the piezoelectric transducer. Besides, within the big dip from 17 to 24 kHz, vibration responses are almost the same for the

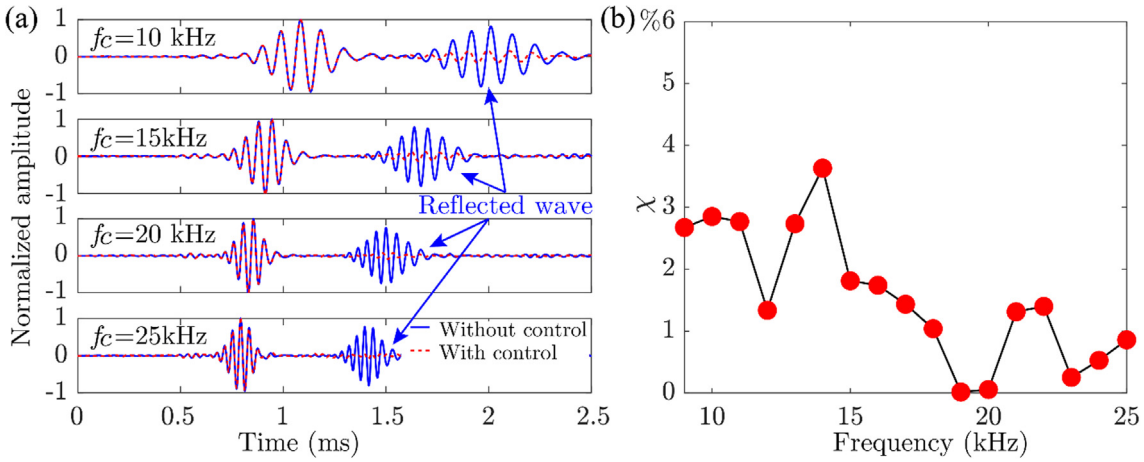

Fig. 3. (a) Experimentally measured time-domain velocity signals from a point on the host beam with control circuits turned ON and OFF. In the tests, central frequencies of incident waves are selected at 10, 15, 20, and 25 kHz. Reflected wave signals are displayed within shaded regions. (b) The difference of absorption coefficients calculated from numerical simulations, A_n, and measured from experiments, A_e, with $\chi = \frac{A_e - A_n}{A_n}$.

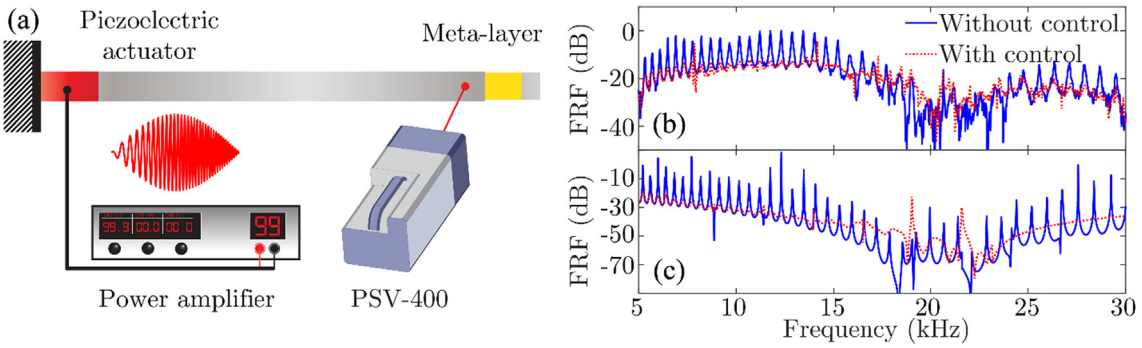

Fig. 4. (a) Experimental setup of the active meta-layer in a cantilever beam for vibration tests. Experimentally tested (b) and numerically calculated (c) Frequency response function (FRF) of the cantilever beam with the active meta-layer connected and disconnected with electrical control circuits.

meta-layer with and without control, which is caused by the position selection of the measured point. Broadband vibration suppression is also validated by numerical simulations shown in Fig. 4(c).

5.3. Vibration suppression of reconfigurable structures

The proposed active meta-layer offers a great advantage in broadband vibration control of reconfigurable structures. In contrast to other approaches based on embedded materials/structures where vibration attenuation performances will be degraded when host structures are deformed, the active meta-layers only occupy on open boundaries of structures and broadband vibration attenuation performances remain when host structures deformed. To demonstrate this, we design a reconfigurable structure with beams connected by elastic thin plates (Fig. 5(a) and (b)) and perform numerical simulations with harmonic loading applied on the structure with two different deformation states. The active meta-layers are attached to the right edges of those beams. In the study, the material used for the beams and thin plates is aluminum. The geometric and material parameters are provided in Tables. 1 and 2, respectively. Fig. 5(c) and (d) show numerically simulated frequency response functions of the two different deformation states. In the figures, displacements at different locations are plotted, when the meta-layer is connected and disconnected with control circuits. It can be clearly seen from the figures that all resonance peaks of passive structures can be effectively suppressed from 5 to 25 kHz when the control circuits in the meta-layers are activated. The results successfully demonstrate the applications of the active meta-layer in broadband vibration control of reconfigurable structures.

5.4. Experimental demonstration of flexural wave cloaking

The cloak is a wave control device that can make objects invisible to waves. Transformation-based passive cloaks constructed by metamaterials are the most popular strategy in manipulating classical waves (i.e. electromagnetic, acoustic, and elastic waves) around objects [45–48]. However, they are usually bulky, imperfection to material damping, and operated at narrow-band frequencies. On the other hand, active cloaks have been proved as an appealing solution in designing broadband, perfect and thin cloaks [49,50]. In light of this, we design and experimentally demonstrate a unidirectional active meta-layer cloak to conceal a void in a plate (Fig. 6(a)). To make the void invisible to flexural waves, active meta-layers surrounding the void are separated into two sections: absorbing (loss) section (blue area) and actuating (gain) section (red area). The meta-layers in the absorbing section facing incident waves are implemented with the optimal transfer function, such that incident waves can be nearly totally absorbed, producing near-zero back scattering. The meta-layers in the actuating section will intentionally regenerate lost (absorbed) waves to the other side of the void through active actuation. The active actuation is controlled by an electrical communication loop, which is connected to the corresponding meta-layer actuator in the absorbing section. The transfer function in the communication loop will produce proper delay so as the actively actuated waves can be projected in the plate in the same way as incident waves propagated in a background plate in the absence of the void, producing cloaking effects.

We then design and fabricate an array of meta-layers in a plate to make a circular void undetectable with flexural waves (Fig. 6(b)). In the following examples, we demonstrate a unidirectional cloak for waves incident from the left side. In the cloak configuration, the left section of the meta-layers behaves as an absorber, and other meta-layers are connected to the absorber accordingly to actively generate flexural waves on the right-hand side of the circular void. An array of piezoelectric transducers are attached on the host plate 185 mm away from the center of the cloak. 10-peak tone-burst signals centered at 15 kHz are applied to the transducers. We apply a Gaussian profile on the amplitudes of those tone-burst signals in order to generate a Gaussian wave beam. The cloaking performance is tested by measuring the out-of-plane velocity wave field around the cloak at different time steps. Fig. 6(c) and (d) show the snapshots of measured velocity fields when the control circuits are deactivated and activated, respectively. Comparing results in two figures, it is seen that the active meta-layer

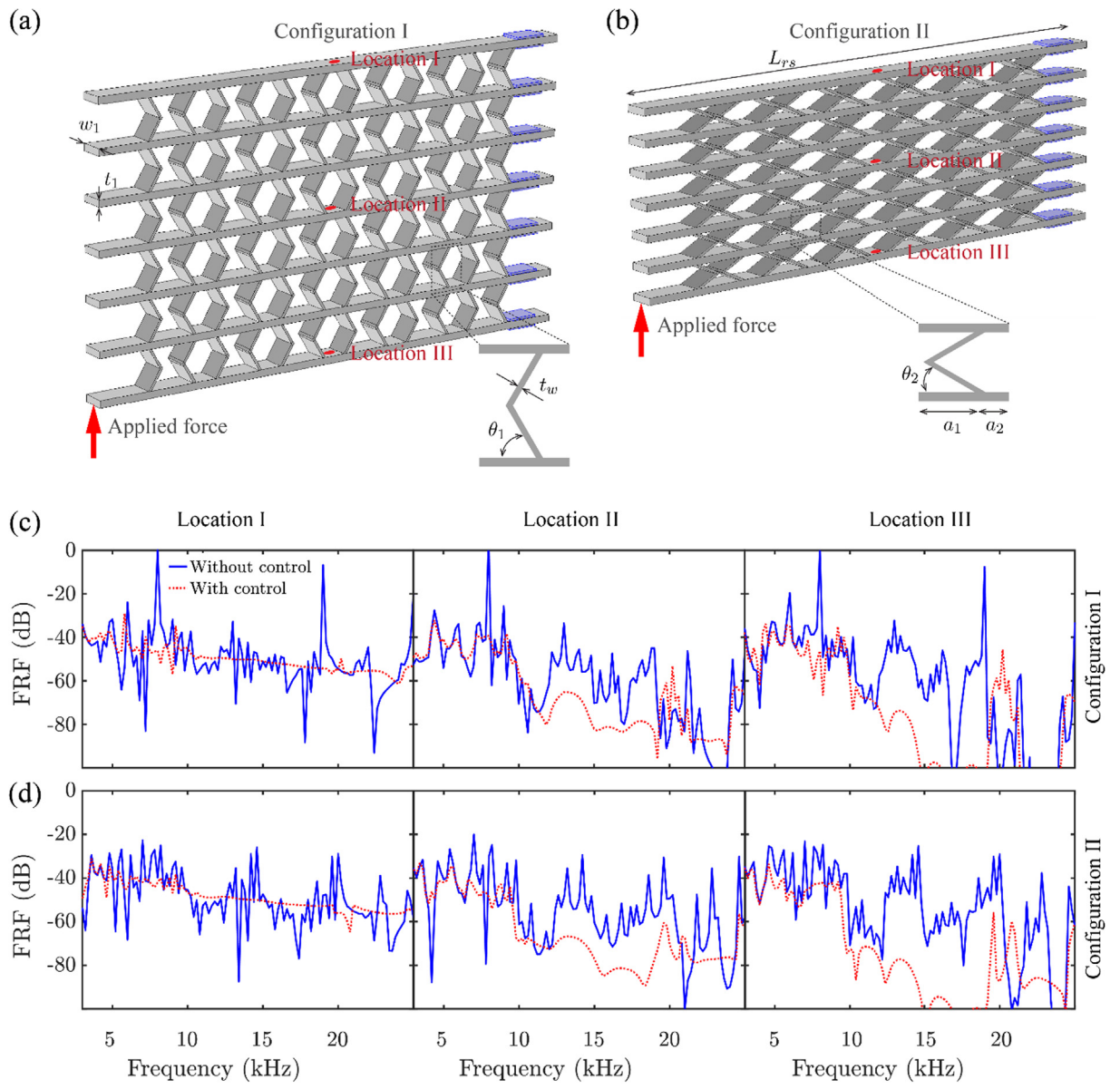

Fig. 5. (a) and (b) Two different deformation states of the reconfigurable structure used in vibration simulations. (c) and (d) Numerically simulated frequency response functions at three different locations of the reconfigurable structure when the active meta-layer is activated (red dotted line) and inactivated (blue solid line). (c): for the deformation state shown in (a); (d): for the deformation state shown in (b). (For interpretation of the references to colour in this figure legend, the reader is referred to the web version of this article.)

manages to suppress the scattering from the void to a high and satisfactory degree although without being perfect. We quantify the cloaking performance by measuring wave amplitudes on two lines in the left and right sides of the cloak at 0.4 and 0.7 ms, respectively (Fig. 6(e) and (f)). It can be clearly seen that waves manipulated by the cloak are very close to that of waves propagated in a background plate in the absence of the void, and backward and forward scattering is trivial, showing nearly perfect cloaking performance. Note that, in the design, the radius of the void is 3.5 times larger than the thickness of the meta-layer, which has been previously considered almost impossible using transformation-based cloaks. Therefore, the active meta-layer cloak holds a great advantage in concealing large objects. In addition, thank to programmable circuits, the reconfigurable meta-layer cloak is also operated at broadband frequencies and conceal objects with different shapes. Numerical simulations are performed to demonstrate cloaking performances of the active meta-layer cloak from the two aspects: (1) The active meta-layer cloak can be operated at different frequencies (see Fig. 7); (2) The active meta-layer cloak can conceal voids with different shapes (see Fig. 8). The geometric and material parameters can be found in Tables 1 and 2, respectively. In Fig. 8(a), the two circular voids are connected with each other creating a new void with complex boundaries.

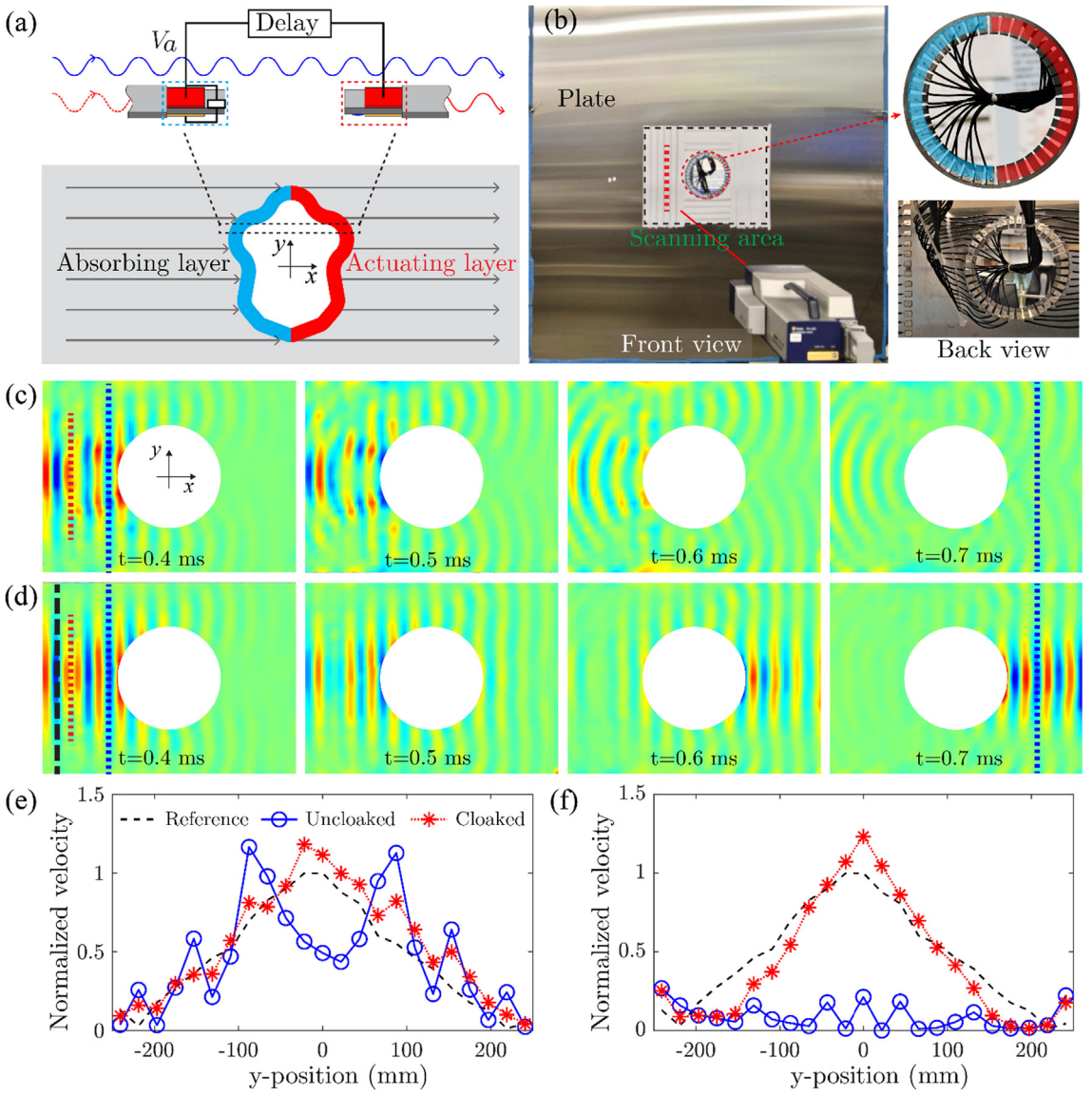

Fig. 6. (a) Working principles of the active meta-layer for flexural wave cloaking of avoid. (b) Fabricated active meta-layers and their experimental setup for flexural wave cloaking. (c) and (d) Experimentally measured out-of-plane velocity wave fields around the meta-layer cloak at different time steps. (c): Control OFF; (d): Control ON. (e) and (f) Experimentally measured normalized velocity fields on two vertical lines (shown in (c) and (d)) in the left and right sides of the meta-layer cloak. (e): x = -116 mm, t = 0.4 ms; (f): x = 150 mm, t = 0.7 ms.

Whereas, in Fig. 8(b), the two circular voids are separated, and the number of voids increases to two. Generally speaking, our approach does not have strong limits in working frequencies, shapes, or sizes of hidden objects.

6. Conclusions

In summary, we design an active meta-layer for realizing an optimal flexural wave absorber. The active meta-layer is composed of piezoelectric sensors and actuators with optimal feedback control loops. The optimal wave absorption performance is formulated and evaluated by an inequality that relates the absorption spectrum and thickness as well as the density of the absorber. We numerically and experimentally demonstrate that the active meta-layer has excellent broadband wave absorption and vibration control abilities in beams and can act as skin cloaks of large voids in plates. In experiments, we apply external wires to connect piezoelectric sensors and actuators with electrical circuits, which in principle could be miniaturized and housed on the meta-layer device itself to maintain the light-weight feature. When employing the meta-layer in engineering applications, it is critical to integrate it in open boundaries of the host medium, which provides a range

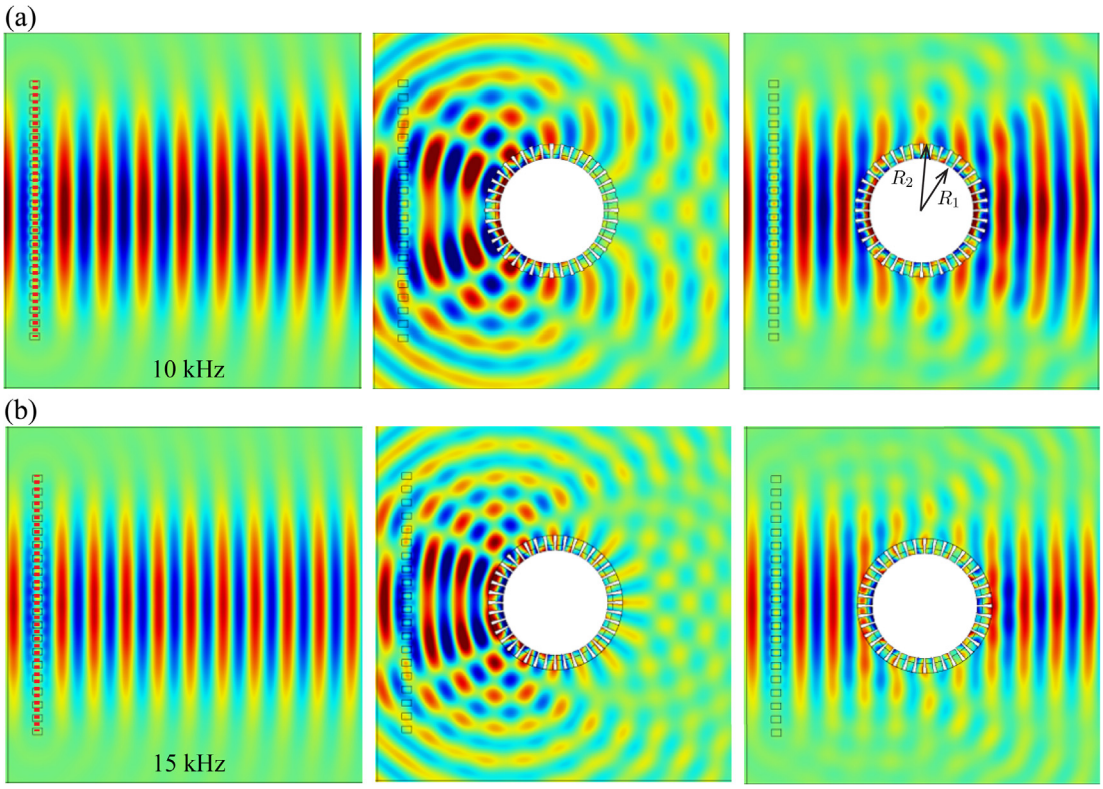

Fig. 7. Numerically simulated out-of-plane displacement wave fields of the active meta-layer cloak. (a) 10 kHz; (b) 15 kHz.

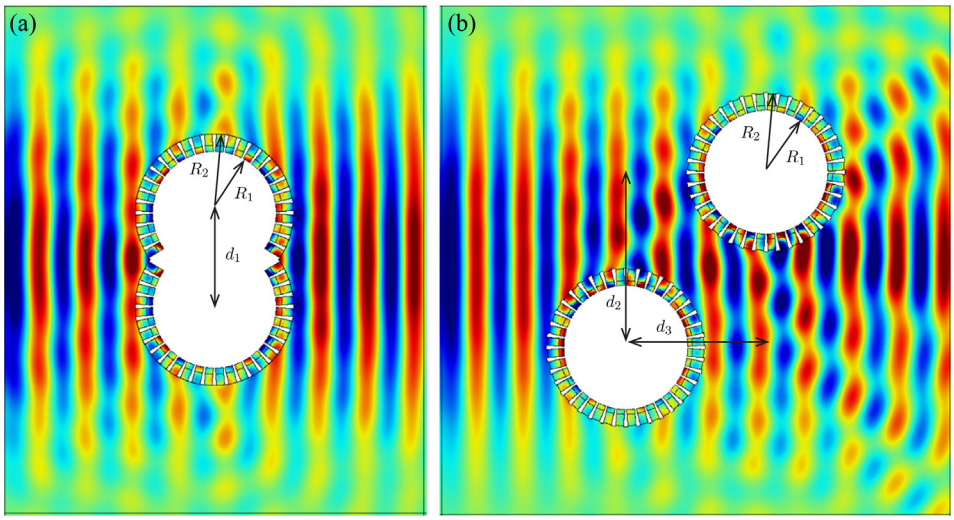

Fig. 8. Numerically simulated out-of-plane displacement wave fields of the active meta-layer cloak with (a) the two circular voids connected with each other creating a new void with complex boundaries and (b) the two circular voids separated, and the number of voids increases to two.

of conveniences in terms of occupation locations and spaces. Thanks to highly reconfigurable properties, the active meta-layer could set the basis of a markedly distinct approach towards perfect absorbers of subwavelength wave and elastic wave cloaking.

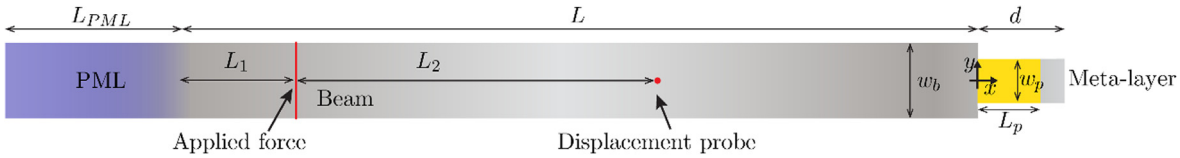

Fig. A1. A simulation model for the beam with an active meta-layer.

Author Contributions

Y.C. and G.H. conceived the concept; X.L. conducted experiments; Y.C. initialized the research and performed theoretical and numerical investigations; Y.C., X.L. and R.Z. discussed modeling and simulation; G.H. supervised the research; All authors wrote the manuscript and interpreted the results.

Declaration of Competing Interest

The authors declare that they have no known competing financial interests or personal relationships that could have appeared to influence the work reported in this paper.

Acknowledgment

This work is supported by the Air Force Office of Scientific Research under Grant No. AF 9550-18-1-0342 with Program Manager Dr. Byung-Lip (Les) Lee.

Appendix. Numerical calculations of ideal transfer functions

To calculate ideal transfer functions at discrete frequencies, we perform a set of numerical simulations according to the derivations in Section 3. Firstly, we numerically evaluate electromechanical coupling coefficients of the sensor and actuator in the meta-layer, κ_s and κ_a, defined in Eqs. (12) and (13). To obtain κ_s, an incident wave is generated from the host beam and propagates to the meta-layer without the electrical connection (refer to Appendix B for details of those harmonic simulations). We then integrate the free charges on the surface of the electrode of the sensor to get the sensing signal V_{sb}, and apply Eq. (13) to retrieve κ_s. To calculate κ_a, we apply a voltage V_a on the actuator of the meta-layer and quantify the amplitude of its generated wave through numerical simulations. κ_a is then able to be retrieved based on Eq. (12). Secondly, we retrieve the transfer function G from the above simulation, where the voltage V_a is applied to the actuator of the meta-layer. By integrating the free charges on the surface of the electrode of the sensor, the feedback voltage V_{fb} can be obtained and the transfer function G is retrieved according to Eq. (13). Thirdly, the passive reflection coefficient r_0 is inferred from two different numerical simulations, where the same incident wave is generated on a homogeneous beam and on a host beam containing a meta-layer without control. Comparing the two wave fields, r_0 can be obtained according to the relation $r_0 = w_r^{(0)}/w_0$. Lastly, by enforcing the reflection coefficient r, the transfer function H can be calculated based on Eq. (15) with the numerically retrieved κ_s, κ_a, G and r_0. The numerical simulation model is shown in Fig. A1 and the corresponding parameters and simulation procedure can be found in Tables 1 and 2 and Appendix B, respectively.

Simulation procedures

Three-dimensional numerical simulations of harmonic waves propagated to the active meta-layer are conducted using the commercial finite element software, COMSOL Multiphysics. In numerical simulations, the 3D linear piezoelectric constitutive law is applied to the piezoelectric patches. The sensing signal is obtained by integrating free charges over a surface of an electrode of the piezoelectric sensor. The two electrodes on the piezoelectric sensor have zero electric potential. The incident flexural wave is generated by applying a transverse force on the host beam. One perfectly matched layers (PMLs) is attached to the other end of the host beam in order to suppress reflected waves from the boundary. One displacement probe is defined on the host beam to measure the out-of-plane displacement and calculate the wave reflection coefficient.

References

[1] G. Ma, P. Sheng, Acoustic metamaterials: From local resonances to broad horizons, Sci. Adv. 2 (2016) e1501595.
[2] S.A. Cummer, J. Christensen, A, Alù, Controlling sound with acoustic metamaterials, Nat. Rev. Mater. 1 (2016) 16001.
[3] M. Haberman, M. Guild, Acoustic metamaterials, Phys. Today 69 (2016) 42–48.
[4] Z. Yang, J. Mei, M. Yang, N.H. Chan, P. Sheng, Membrane-type acoustic metamaterial with negative dynamic mass, Phys. Rev. Lett. 101 (2008) 204301.
[5] Y.Y. Chen, M.V. Barnhart, J.K. Chen, G.K. Hu, C.T. Sun, G.L. Huang, Dissipative elastic metamaterials for broadband wave mitigation at subwavelength scale, Compos. Struct. 136 (2016) 358–371.

[6] D.L. Yu, Y.Z. Liu, G. Wang, H.G. Zhao, J. Qiu, Flexural vibration band gaps in Timoshenko beams with locally resonant structures, J. Appl. Phys. 100 (2006) 124901.
[7] X. Li, Y. Chen, G. Hu, G. Huang, A self-adaptive metamaterial beam with digitally controlled resonators for subwavelength broadband flexural wave attenuation, Smart Mater. Struct. 27 (2018) 45015.
[8] G. Trainiti, Y. Ra'di, M. Ruzzene, A. Alù, Coherent virtual absorption of elastodynamic waves, Sci. Adv. 5 (2019), eaaw3255.
[9] D. Misseroni, D.J. Colquitt, A.B. Movchan, N.V. Movchan, I.S. Jones, Cymatics for the cloaking of flexural vibrations in a structured plate, Sci. Rep. 6 (2016) 23929.
[10] M. Miniaci, R.K. Pal, B. Morvan, M. Ruzzene, Experimental observation of topologically protected helical edge modes in patterned elastic plates, Phys. Rev. X 8 (2018) 031074.
[11] M. Miniaci, R.K. Pal, R. Manna, M. Ruzzene, Valley-based splitting of topologically protected helical waves in elastic plates, Phys. Rev. B 100 (2019) 024304.
[12] R. Fleury, D. Sounas, A. Alu, An invisible acoustic sensor based on parity-time symmetry, Nat. Commun. 6 (2015) 1–7.
[13] X. Zhu, H. Ramezani, C. Shi, J. Zhu, X. Zhang, P t-symmetric acoustics, Phys. Rev. X 4 (2014) 031042.
[14] Y. Chen, G. Hu, G. Huang, A hybrid elastic metamaterial with negative mass density and tunable bending stiffness, J. Mech. Phys. Solids. 105 (2017) 179–198.
[15] R. Zhu, Y.Y. Chen, M.V. Barnhart, G.K. Hu, C.T. Sun, G.L. Huang, Experimental study of an adaptive elastic metamaterial controlled by electric circuits, Appl. Phys. Lett. 108 (2016) 11905.
[16] P. Celli, S. Gonella, Tunable directivity in metamaterials with reconfigurable cell symmetry, Appl. Phys. Lett. 106 (2015) 91905.
[17] G. Wang, J. Cheng, J. Chen, Y. He, Multi-resonant piezoelectric shunting induced by digital controllers for subwavelength elastic wave attenuation in smart metamaterial, Smart Mater. Struct. 26 (2017) 25031.
[18] K. Yi, M. Ouisse, E. Sadoulet-Reboul, G. Matten, Active metamaterials with broadband controllable stiffness for tunable band gaps and non-reciprocal wave propagation, Smart Mater. Struct. 28 (2019) 65025.
[19] H. Zhu, T.F. Walsh, F. Semperlotti, Experimental study of vibration isolation in thin-walled structural assemblies with embedded total-internal-reflection metasurfaces, J. Sound Vib. 456 (2019) 162–172.
[20] Y. Li, B.M. Assouar, Acoustic metasurface-based perfect absorber with deep subwavelength thickness, Appl. Phys. Lett. 108 (2016) 063502.
[21] K. Donda, Y. Zhu, S.W. Fan, L. Cao, Y. Li, B. Assouar, Extreme low-frequency ultrathin acoustic absorbing metasurface, Appl. Phys. Lett. 115 (2019) 173506.
[22] J. Mei, Y. Wu, Controllable transmission and total reflection through an impedance-matched acoustic metasurface, New J. Phys. 16 (2014) 123007.
[23] H. Zhu, F. Semperlotti, Anomalous refraction of acoustic guided waves in solids with geometrically tapered metasurfaces, Phys. Rev. Lett. 117 (2016) 034302.
[24] Y. Li, X. Jiang, R.Q. Li, B. Liang, X.Y. Zou, L.L. Yin, J.C. Cheng, Experimental realization of full control of reflected waves with subwavelength acoustic metasurfaces, Phys. Rev. Applied 2 (2014) 064002.
[25] Y. Liu, Z. Liang, F. Liu, O. Diba, A. Lamb, J. Li, Source illusion devices for flexural lamb waves using elastic metasurfaces, Phys. Rev. Lett. 119 (2017) 034301.
[26] S. Li, J. Xu, J. Tang, Tunable modulation of refracted lamb wave front facilitated by adaptive elastic metasurfaces, Appl. Phys. Lett. 112 (2018) 021903.
[27] Y. Chen, X. Li, H. Nassar, G. Hu, G. Huang, A programmable metasurface for real time control of broadband elastic rays, Smart Mater. Struct. 27 (2018) 115011.
[28] M.J. Brennan, Control of flexural waves on a beam using a tunable vibration neutraliser, J. Sound Vib. 222 (1999) 389–407.
[29] M.J. Brennan, Vibration control using a tunable vibration neutralizer, Proc. Inst. Mech. Eng. Part C J. Mech. Eng. Sci. 211 (1997) 91–108.
[30] B.C. Nakra, Vibration control in machines and structures using viscoelastic damping, J. Sound Vib. 211 (1998) 449–466.
[31] C. Huang, J. Yao, T. Zhang, Y. Chen, H. Jiang, D. Li, Damping applications of ferrofluids: a review, J. Magn. 22 (2017) 109–121.
[32] Y.-J. Liang, L.-W. Chen, C.-C. Wang, I.-L. Chang, An acoustic absorber implemented by graded index phononic crystals, J. Appl. Phys. 115 (2014) 244513.
[33] Y. Jin, B. Djafari-Rouhani, D. Torrent, Gradient index phononic crystals and metamaterials, Nanophotonics. 8 (2019) 685–701.
[34] E. Kim, R. Chaunsali, J. Yang, Gradient-index granular crystals: From boomerang motion to asymmetric transmission of waves, Phys. Rev. Lett. 123 (2019) 214301.
[35] V. Denis, F. Gautier, A. Pelat, J. Poittevin, Measurement and modelling of the reflection coefficient of an Acoustic Black Hole termination, J. Sound Vib. 349 (2015) 67–79.
[36] V.B. Georgiev, J. Cuenca, F. Gautier, L. Simon, V.V. Krylov, Damping of structural vibrations in beams and elliptical plates using the acoustic black hole effect, J. Sound Vib. 330 (2011) 2497–2508.
[37] Y.-K. Kim, H.-I. Bae, J.-H. Koo, K.-S. Kim, S. Kim, Note: Real time control of a tunable vibration absorber based on magnetorheological elastomer for suppressing tonal vibrations, Rev. Sci. Instrum. 83 (2012) 46108.
[38] C.L. Davis, G.A. Lesieutre, An actively tuned solid-state vibration absorber using capacitive shunting of piezoelectric stiffness, J. Sound Vib. 232 (2000) 601–617.
[39] P.L. Walsh, J.S. Lamancusa, A variable stiffness vibration absorber for minimization of transient vibrations, J. Sound Vib. 158 (1992) 195–211.
[40] N. Olgac, B.T. Holm-Hansen, A novel active vibration absorption technique: delayed resonator, J. Sound Vib. 176 (1994) 93–104.
[41] K.N. Rozanov, Ultimate thickness to bandwidth ratio of radar absorbers, IEEE Trans. Antennas Propag. 48 (2000) 1230–1234.
[42] M. Yang, S. Chen, C. Fu, P. Sheng, Optimal sound-absorbing structures, Mater. Horizons. 4 (2017) 673–680.
[43] M. Kuzuoglu, R. Mittra, Frequency dependence of the constitutive parameters of causal perfectly matched anisotropic absorbers, IEEE Microw. Guid. Wave Lett. 6 (1996) 447–449.
[44] K.R. Waters, J. Mobley, J.G. Miller, Causality-imposed (Kramers-Kronig) relationships between attenuation and dispersion, IEEE Trans. Ultrason. Ferroelectr. Freq. Control. 52 (2005) 822–823.
[45] H. Shen, M.P. Païdoussis, J. Wen, D. Yu, L. Cai, X. Wen, Acoustic cloak/anti-cloak device with realizable passive/active metamaterials, J. Phys. D. Appl. Phys. 45 (2012) 285401.
[46] M. Farhat, S. Guenneau, S. Enoch, A.B. Movchan, Cloaking bending waves propagating in thin elastic plates, Phys. Rev. B. 79 (2009) 33102.
[47] M. Farhat, S. Guenneau, S. Enoch, Ultrabroadband elastic cloaking in thin plates, Phys. Rev. Lett. 103 (2009) 24301.
[48] N. Stenger, M. Wilhelm, M. Wegener, Experiments on elastic cloaking in thin plates, Phys. Rev. Lett. 108 (2012) 14301.
[49] H. Li, M. Rosendo-López, Y. Zhu, X. Fan, D. Torrent, B. Liang, J. Cheng, J. Christensen, others, Ultrathin acoustic parity-time symmetric metasurface cloak, Research. 2019 (2019) 8345683.
[50] D.L. Sounas, R. Fleury, A. Alù, Unidirectional cloaking based on metasurfaces with balanced loss and gain, Phys. Rev. Appl. 4 (2015) 14005.